Human Molecular Genetics, 2005, Vol. 14, No. 24 ***3787–3799***
doi:10.1093/hmg/ddi393
Advance Access published on October 20, 2005

Frataxin deficiency alters heme pathway transcripts and decreases mitochondrial heme metabolites in mammalian cells

Robert A. Schoenfeld[1,†], Eleonora Napoli[1,†], Alice Wong[1], Shan Zhan[1], Laurence Reutenauer[5], Dexter Morin[1], Alan R. Buckpitt[1], Franco Taroni[2], Bo Lonnerdal[3], Michael Ristow[4], Hélène Puccio[5] and Gino A. Cortopassi[1,*]

[1]Department of Molecular Biosciences, [2]Department of Nutrition, University of California, Davis, USA, [3]Division of Biochemistry and Genetics, Instituto Nazionale Neurologico, Carlo Besta, Via Celoria 11, Milan, Italy, [4]Department of Human Nutrition, Institute of Nutrition, University of Jena, Germany and [5]Institut de Génétique et de Biologie Moléculaire et Cellulaire, CNRS/INSERM/Université Louis Pasteur, Strasbourg, France

Received August 18, 2005; Revised and Accepted October 13, 2005

Deficiency of the frataxin mRNA alters the transcriptome, triggering neuro- and cardiodegeneration in Friedreich's ataxia. We microarrayed murine frataxin-deficient heart tissue, liver tissue and cardiocytes and observed a transcript down-regulation to up-regulation ratio of nearly 2:1 with a mitochondrial localization of transcriptional changes. Combining all mouse and human microarray data for frataxin-deficient cells and tissues, the most consistently decreased transcripts were mitochondrial coproporphyrinogen oxidase (CPOX) of the heme pathway and mature T-cell proliferation 1, a homolog of yeast COX23, which is thought to function as a mitochondrial metallochaperone. Quantitative RT-PCR studies confirmed the significant down-regulation of Isu1, CPOX and ferrochelatase at 10 weeks in mouse hearts. We observed that mutant cells were resistant to aminolevulinate-dependent toxicity, as expected if the heme pathway was inhibited. Consistent with this, we observed increased cellular protoporphyrin IX levels, reduced mitochondrial heme *a* and heme *c* levels and reduced activity of cytochrome oxidase, suggesting a defect between protoporphyrin IX and heme *a*. Fe-chelatase activities were similar in mutants and controls, whereas Zn-chelatase activities were slightly elevated in mutants, supporting the idea of an altered metal-specificity of ferrochelatase. These results suggest that frataxin deficiency causes defects late in the heme pathway. As ataxic symptoms occur in other diseases of heme deficiency, the heme defect we observe in frataxin-deficient cells could be primary to the pathophysiological process.

INTRODUCTION

Friedreich's ataxia (FRDA) is the most commonly inherited recessive ataxia, striking approximately one in 50 000 (1). FRDA pathology includes neurodegeneration of the large sensory neurons and spinocerebellar tracts, cardiomyopathy, impaired glucose tolerance and diabetes mellitus. The age of onset is variable; mild cases are occasionally observed, but reduced life expectancy is the norm. The progression of the disease has been elucidated using mouse knockout models (2,3).

FRDA results from reduced expression of frataxin, a nuclear encoded gene of controversial function. This reduction is caused by an expanded GAA repeat in the first intron of the gene (4). Expanded strands can form triple helices and associate to form 'sticky DNA' complexes, which partially inhibit transcription elongation (5–8). The severity of the disease is proportional to the length of the expansion (9–13).

*To whom correspondence should be addressed at: Department of Molecular Biosciences, 1 Shields Avenue, Davis, CA 95616, USA. Tel: +1 5307549665; Fax: +1 5307549342; Email: gcortopassi@ucdavis.edu
†The authors wish it to be known that, in their opinion, the first two authors should be regarded as joint First Authors.

Frataxin's roles in iron–sulfur cluster functions

The precise function of frataxin has been unclear, but a role in iron–sulfur cluster (ISC) biosynthesis and repair or in enhancing in iron bioavailability, has been suggested (14). Additionally, recombinant frataxins have been shown to interact with the IscU and the iron–sulfur proteins, ferrochelatase and mitochondrial aconitase (15–18).

Numerous studies have shown that frataxin plays a role in ISC biosynthesis and maintenance. Experiments in yeast have shown that the yeast frataxin homolog YHF1 interacts with the iron–sulfur scaffold protein Isu1 and the cysteine desulfurase Nsf1, and depletion of YFH1 reduces the maturation of ISC proteins (19–23). Microarray analysis of human cells has shown that frataxin depletion affects ISC transcripts preferentially (24), and a recent study in human cells demonstrated that the ISC enzyme impairment was an early effect of frataxin deficiency (25). At high concentration, frataxin can oligomerize into large complexes which bind iron (26–30) and a putative iron-binding site has been mapped in the yeast and bacterial homologs (31,32).

Frataxin and heme

Several recent studies in yeast have shown a frataxin-dependent effect on heme biosynthesis. Lesuisse *et al.* (33) demonstrated that Fe–protoporphyrin IX levels were reduced in Δ*yfh1* mutants, whereas Zn–protoporphyrin IX levels were elevated. Lange *et al.* (34) demonstrated reduced heme synthesis in yeast mutated in various components of the ISC biosynthetic pathway, including Δ*yfh1*.

The heme pathway is of particular interest in the pathology of FRDA because the terminal step in this pathway involves both iron handling and an ISC protein. Ferrochelatase, the final enzyme in the heme biosynthetic pathway, incorporates iron into protoporphyrin IX. It is an ISC protein in mammals, but not in yeast (35). Multiple studies have demonstrated a physical interaction between frataxin and ferrochelatase (16,17,33).

We have previously performed microarray analysis on human cells derived from FRDA patients. In this study, we have expanded on those results by performing microarray analysis on frataxin-deficient mouse hearts (2), cardiocytes and liver/hepatocytes. By combining murine and human results, we determined that, second to frataxin, the coproporphyrinogen oxidase and mature T-cell proliferation 1 transcripts were decreased within the largest number of mutant samples, suggesting an alteration in the heme pathway. We further demonstrate functional and biochemical alterations of the heme pathway and cytochrome oxidase and discuss these in terms of frataxin function and possible FRDA therapy.

RESULTS

Microarray analysis of frataxin-deficient mouse tissues

Microarray analysis was performed on four sets of frataxin-deficient mouse tissues. Two sets were heart tissue taken from 5- and 10-week-old mice in which frataxin was disrupted using the muscle creatine kinase promoter (2). Another set was derived from mice in which frataxin was specifically disrupted in murine hepatocytes (M. Ristow, unpublished data). The final set was derived from HL-1 mouse cardiocytes (36) transiently transfected with frataxin siRNA. Quantitative RT-PCR (QRTPCR) analysis confirmed a decrease in the frataxin transcript (data not shown).

Table 1. Microarray results from frataxin-deficient mouse tissues

Sample	Number of unique altered genes	Number of unique up-regualted	Number of unique down-regulated
5 week heart KO	441	175	266
10 week heart KO	857	450	407
HL-1 frataxin RNAi	1554	556	998
3 month liver KO	1539	427	1112
All samples	3969	1349	2347

Redundant probsets (representing the same gene) have been eliminated from the analysis and only unique gene names were counted. As many unique genes were significantly altered in multiple samples, the number of "all samples" do not reflect the sum total of individual samples.

Each data set was analyzed individually using dChip (37). A total of 3696 unique genes were significantly altered in at least one data set. Of these, 2347 were down-regulated and 1349 were up-regulated (Table 1). Thus, frataxin deficiency had a repressive effect on the transcriptome by a ratio of almost 2:1.

Frataxin produces a statistically significant alteration in mitochondrial-specific transcripts

Significantly, altered transcripts were analyzed with respect to cellular compartment, using the program Onto-Express (38). The mitochondrial compartment was the only one to be significantly altered in all comparisons ($n = 4$), and the average corrected P-value was highly significant ($P = 0.00004$, Table 2). A total of 54 mitochondrial genes were identified in this analysis. Of these, 44 were down-regulated and 10 were up-regulated (data not shown). Thus, conditional or complete knockout of frataxin in mouse tissues produces a highly significant and repressive effect on mitochondrial transcripts.

Frataxin deficiency across cell types and species causes deficiency of CPOX and MTCP1 transcripts

One way to identify the root causes of the observed mitochondrial-specific repression was to identify the broadest transcriptomal consequences of frataxin deficiency across species and cell types. To this end, we combined the mouse microarray data with human data on frataxin-deficient cells (24). Significantly, altered mouse genes were cross-referenced for human orthologs, using the Affymetrix NetAffx database (39), and the combined list was filtered for transcripts with significantly altered expression at the $P < 0.05$ criterion, altered in the same direction and present in at least two data sets. A total of 1132 transcripts satisfied these criteria, of which only the transcripts shared in more than four comparisons are shown (Table 3).

The most consistent consequence of frataxin deficiency in mouse and human cells aside from the deficiency of frataxin

Table 2. Cell component cluster analysis of mouse microarray results

Cellular compartment	H5	H10	HL1	L	Average corrected *P*
Mitochondrion	3.25E−05	9.33E−05	3.03E−05	3.04E−15	3.90E−05
Extracellular space	9.29E−03	NS	4.49E−06	9.49E−05	3.13E−03

Figures refer to corrected *P* values. NS, not statistically significant. Only categories present in three or more samples are shown. H5, 5 week heart knockout; H10, 10 week heart knockout; HL1, HL-1 cells transfected with frataxin siRNA; L, 3 month liver knockout.

transcript itself was an inhibition of two mitochondrial transcripts: coproporphyrinogen oxidase (CPOX) and mature T-cell proliferation 1 (MTCP1). Both transcripts appeared in six out of eight samples and were down-regulated. Cystatin B, mutations in which cause myoclonic epilepsy (40) and which has been proposed to form protein aggregates to cause neurological disease (41), was up-regulated in 5/8 samples. Rhodanese, which functions in repair of Fe–S proteins, was down-regulated in 4/8 samples.

Confirmation of heme transcript decrease in frataxin-deficient mouse hearts and human lymphoblasts

The coproporphyrinogen oxidase transcript encodes mitochondrial coproporphyrinogen oxidase (CPOX), a heme biosynthetic enzyme which has been identified as a regulatory step in the heme pathway (42). We confirmed that CPOX transcript levels were consistently decreased, using QRTPCR in human lymphoblasts (data not shown). Other iron–sulfur and heme-related transcripts were investigated by QRTPCR in 3-, 5-, and 10-week frataxin-deficient mouse hearts (2), including Isu1, CPOX, ALAS1 and ferrochelatase. Isu1, CPOX and ferrochelatase each showed a significant down-regulation at 10 weeks (Fig. 1). Additionally, a significant down-regulation of ferrochelatase transcript was observed in 7- and 8-week frataxin-deficient hearts.

Functional down-regulation of the heme biosynthetic pathway in human cells

The heme biosynthetic pathway converts δ-aminolevulinate to the phototoxic product protoporphyrin IX (43). Thus, if the transcriptional repression of coproporphyrinogen oxidase we observe by microarray and QRTPCR has a significant effect on pathway flux, we would predict mutant cells to be resistant to the phototoxic consequences of δ-aminolevulinate exposure. FRDA and control lymphoblasts were challenged with δ-aminolevulinate (ALA) for 0–30 min, then exposed to 400–410 nm (blue) light for 5 min. Although both mutant and control cells were sensitized to blue light in a time- and dose-dependent manner, FRDA cells were significantly ($P < 0.05$) more resistant to blue light than controls at early time points, i.e. 30 min after feeding the cells 300 μM ALA (Fig. 2). At later time points, this difference became non-significant, suggesting a kinetic inhibition of the pathway rather than an absolute block.

Table 3. Significantly altered transcripts appearing in four or more tissues

Gene title	Symbol	Function	Count	Compartment	Mouse			Human				Average FC	Average *P*
					H5	H10	HL1	L	F	LyT	Ly	NT2	
Friedreich ataxia	Frda	Frataxin	7/8	Mitochondrion	−1.5	−1.8	−1.4		−1.1	−1.7	−1.4	−2.5	−1.61	0.0233
Coproporphyrinogen oxidase	Cpox	Heme	6/8	Mitochondrion	−1.2	−1.5	−1.8	−1.6		−1.6	−1.5		−1.53	0.0193
Mature T-cell proliferation 1	Mtcp1	Cu delivery	6/8	Mitochondrion	−1.3	−1.4	−2.6		−1.2	−1.2	−1.3		−1.50	0.0166
Cystatin B	Cstb	Protease inhibitor	5/8	Cytoplasm	1.5	4.5	1.6	3.4		1.8			2.54	0.0227
Cadherin 2	Cdh2	Cell adhesion	4/8	Cell membrane		−1.7	−2.7	−1.8	−5.6				−2.92	0.0081
CD59a antigen	Cd59a	Complement	4/8	Mitochondrion	−1.4	−2.2	−4.9	−1.9					−2.62	0.0063
DEAD box polypeptide 1	Ddx1	RNA splicing	4/8	Nucleus	1.2		2.5	1.6			1.2		1.60	0.0296
Cardiolipin acyltransferase	AlCat1	Cardiolipin metab.	4/8	ER	−1.5	−2.6	−1.3	−1.4					−1.71	0.200
Kinesin family memebr 1C	Kif1c	Microtubule	4/8	Golgi	−1.4	−2.1	−1.6	−1.6					−1.68	0.0150
L-3-HA-CoA DH, short chain	Hadhsc	Beta-oxidation	4/8	Mitochondrion	−1.1			−2.3		−1.3		−1.3	−1.49	0.0112
Major vault protein	Mvp	Drug resistance	4/8	Cytoplasm	1.2	1.6			1.3	1.6			1.43	0.0188
Phosphatidylserine synthase 1	Ptdss1	PS synthesis	4/8	Mitochondrion		−1.2		−1.4		−1.3	−1.2		−1.28	0.288
SWI/SNF related	Smarca2	Gene regulation	4/8	Nucleus			−1.9	−1.6		−1.6	−1.5		−1.67	0.0095
Rhodanese, mitochondrial	Tst	ISC protein maint.	4/8	Mitochondrion			−1.70	−1.40		1.70	−1.60		−1.57	0.0101

Figures refer to fold change (frataxin deficient/control). H5, 5 week heart knockout; H10, 10 week heart knockout; HL1, HL-1 cells transfected with frataxin siRNA; L, 3 month liver knockout; F, fibroblasts; LyT, FRDA patient lymphoblasts transfected with frataxin; Ly, lymphoblasts; NT2, cells transfected with frataxin RNAi.

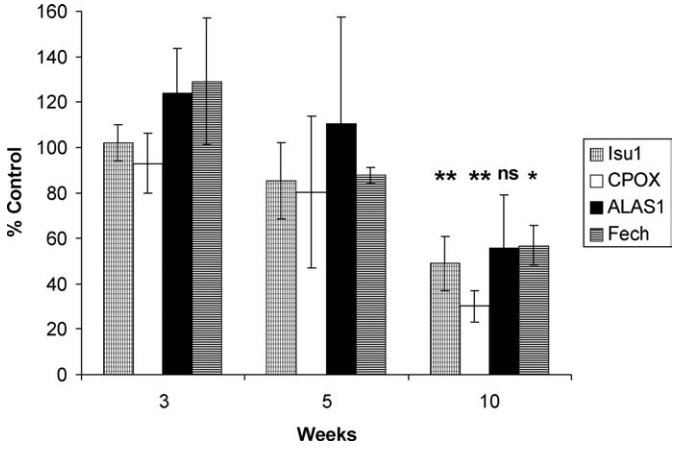

Figure 1. QRTPCR results of iron–sulfur and heme-related transcripts from 3-, 5- and 10-week frataxin-deficient mice. Isu1, iron–sulfur scaffold 1; ALAS1, aminolevulinate synthase 1; FECH, ferrochelatase; CPOX, coproporphyrinogen oxidase. Error bars indicate standard deviation. $^{*}P \leq 0.05$; $^{**}P \leq 0.001$; ns, not significant.

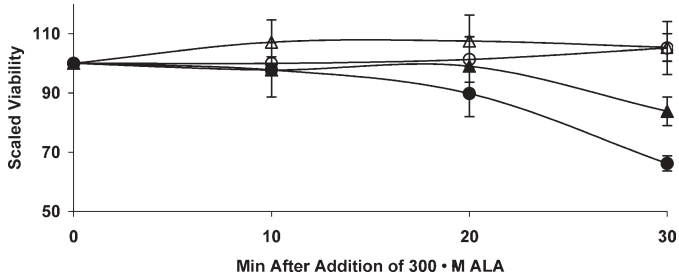

Figure 2. FRDA lymphoblasts are less photosensitive to a 5 min blue light exposure than controls following challenge with 300 μM ALA. Viability is scaled to cell viability immediately following addition of ALA. Results are expressed as mean ± SEM for three controls and three FRDA mutants. –○– Controls. no light: – ● – controls + blue light; –△–FRDA, no light; –▲– FRDA + blue light.

Buildup of protoporphyrin IX and decrease in hemes *a* and *c* in mutant mitochondria

If frataxin causes inhibition of the heme pathway, one might expect increases in heme metabolite levels upstream of the inhibited step and decreased metabolite levels downstream of the inhibited step (Fig. 3). Using HPLC, we investigated the levels of protoporphyrin IX and heme *b* in cellular extracts and heme *a* and heme *b* in mitochondrial extracts of human lymphoblasts. Protoporphyrin IX and heme *b* were elevated by ~3.5-fold in cellular extracts of mutants (Fig. 4A and B), consistent with a defect downstream of PpIX in the heme pathway. Although total cellular heme *b* levels were increased in mutants by ~3.5-fold, mitochondrial heme *b* levels were not increased, i.e. they were not significantly different in mutants and controls (Fig. 4C). In contrast, the ratio of mitochondrial heme *b* to heme *a* was significantly increased in mutants (Fig. 4D), i.e. mitochondrial heme *a* levels were significantly decreased relative to mitochondrial heme *b*. Thus, frataxin deficiency results in a deficiency in mitochondrial heme *a*, an essential cofactor for cytochrome oxidase. We also observed a frataxin-dependent defect in heme *c* levels (discussed subsequently).

Alteration in Zn-chelatase but not Fe-chelatase activity

Given the earlier indications of a heme pathway inhibition and the fact that ferrochelatase is an ISC protein in humans, we studied the activity of ferrochelatase to insert either iron (i.e. Fe-chelatase) or zinc (Zn-chelatase) into protophorphyrin IX in human lymphoblasts. Although we observed Fe-chelatase activity in mitochondrial extracts, which was completely inhibitable by the ferrochelatase inhibitor *N*-methyl protoporphyrin IX, we observed no significant decrease in the mean and median Fe-chelatase activity in mitochondrial extracts of mutant extracts (Fig. 5A), consistent with another study (34). In contrast, we did observe a small but significant increase in mutant Zn-chelatase activity (Fig. 5B). There was no difference in ferrochelatase protein concentration in mutants versus controls, demonstrating that the increased Zn-chelatase activity was not the result of altered protein amount (Fig. 5C). These data suggest that the defect in heme *a* and *c* production is not the direct result of a defective Fe-chelatase activity of ferrochelatase. The small increase in Zn-chelatase activity suggests that one of frataxin's functions may be to deliver iron to ferrochelatase and that under conditions of frataxin deficiency, ferrochelatase becomes less selective for iron insertion into PpIX.

Deficient heme *c* levels in cytochrome *c* of mutant cells

The heme pathway is split, in that heme *b* is a precursor for both heme *a*, which is inserted into cytochrome oxidase, and heme *c*, which is inserted into cytochrome *c* (Fig. 3). We assayed heme *c* insertion into cytochrome *c* by the *ortho*-dianisidine heme stain and by western blot of human lymphoblasts (Fig. 6). Frataxin deficiency results in lower heme *c* staining by ~40% (Fig. 6A), and frataxin expression is significantly correlated with heme *c* levels (Fig. 6E). Frataxin deficiency results in a decreased expression of mitochondrial cytochrome *c* protein (Fig. 6B), by ~15%. However, when normalized for cytochrome *c* levels, frataxin deficiency results in a further decrease of heme *c* insertion into cytochrome *c*, by ~27%. Thus, the decreased heme *c* level in mutants is the result of two factors, less cytochrome *c* and deficient loading of heme *c* onto cytochrome *c*.

MTCP1 is a homolog of the COX17/COX23 cytochrome oxidase assembly protein

The other transcript down-regulated in frataxin-deficient cells as often as CPOX was MTCP1, i.e. in 6/8 comparisons. MTCP1 is located at a chromosomal breakpoint that occurs in T-cell leukemias and ataxia-telangiectasia and is thought to be involved in cell proliferation (44). The p8 isoform has a mitochondrial localization (45) and a novel protein structure (46).

We compared the $p8^{MTCP1}$ protein sequence against all known yeast genes using BLASTP (47). The top matches were to three mitochondrial proteins: COX23, MRP10 and COX17. COX23 and COX17 are transport proteins located

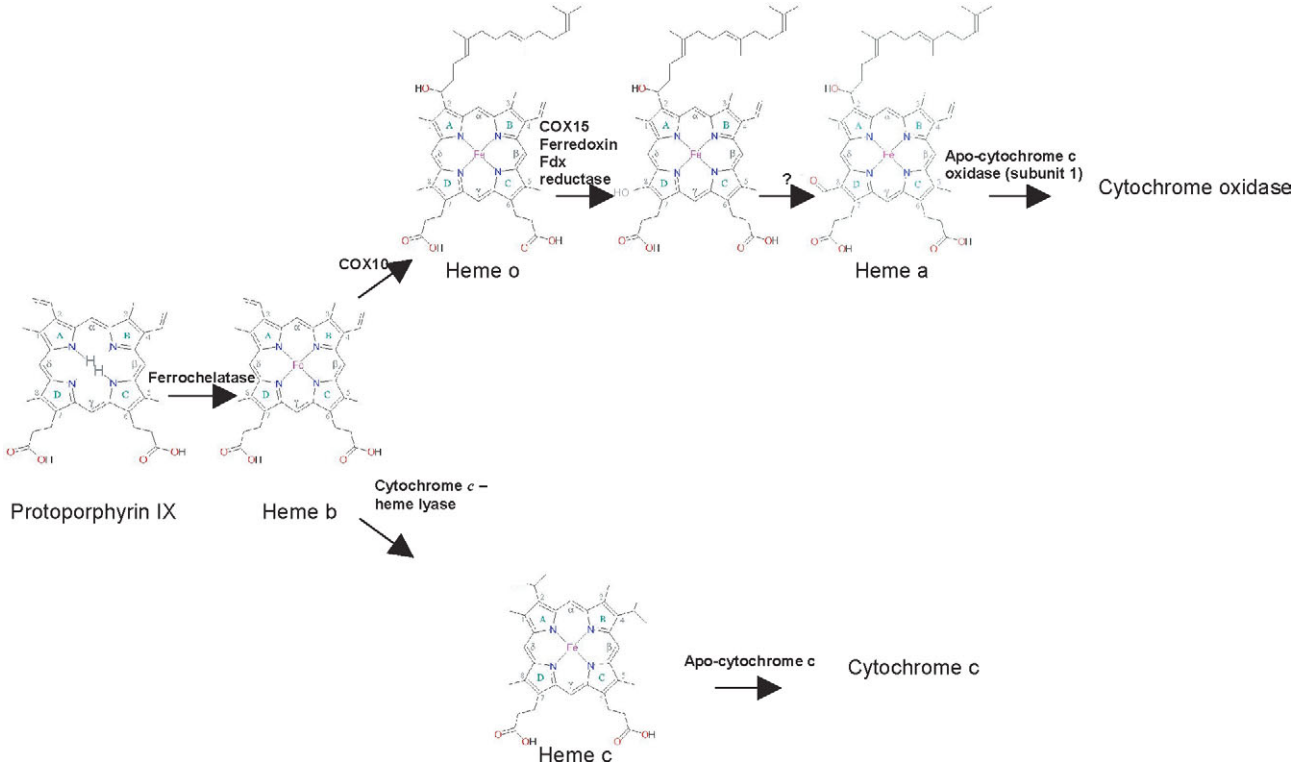

Figure 3. Origin of hemes for mitochondrial hemoproteins. Heme *b* is converted to either heme *a* and inserted into cytochrome oxidase or heme *c* and inserted into cytochrome *c*. Adapted from Moraes *et al.* (68) and Bertini (69).

in the mitochondrial intermembrane space and are thought to function together as metallochaperones for the delivery of copper to cytochrome oxidase (48). Sequence alignments between MTCP1, COX17, COX23 and several other proteins involved in cytochrome oxidase assembly demonstrated that COX23 had the lowest distance score, whereas other cytochrome oxidase assembly proteins and the putative iron carrier protein MRS3 had higher scores (Figs 7A and B). For comparison, an unrelated yeast protein, histone protein Hht2p, had the highest distance score (Fig. 7B). Structural alignments of p8^{MTCP1} and COX17 generated with Cn3D (49) demonstrate that both molecules have a common loop structure (Fig. 7B). COX17 and COX23 interact with SCO1 and SCO2, mutations in which cause cytochrome oxidase deficiency in humans (50,51). If MTCP1 is a functional homolog of COX23/17, this (along with the deficient heme *a* observed earlier) suggests that frataxin deficiency should cause cytochrome oxidase deficiency.

Cytochrome *c* oxidase activity, but not protein level of COX subunit I or II, is decreased in frataxin-deficient lymphoblasts

We demonstrated that mitochondrial heme *b*/heme *a* ratio is significantly increased in mutants, whereas mitochondrial heme *b* levels are not significantly different, thus heme *a* levels are decreased (Fig. 4). Heme *a* is an essential component of cytochrome oxidase (COX). In addition, if the MTCP1 transcript is in fact the homolog of COX17/23 as our analysis suggests, the assembly or function of cytochrome oxidase should decrease, as is observed in COX17/23-deficient yeast (52). In fact, we observed that cytochrome oxidase (Complex IV) activity was significantly decreased in frataxin-deficient human lymphoblasts by a mean level of 27% when compared with controls ($P < 0.005$, Fig. 8D). In contrast, Complex I activity was unchanged, Complex III activity was significantly increased by ~45% and Complex II activity was decreased by ~30% (Figs 8A–C). We observed a significant correlation between frataxin levels and Complex IV activity ($P < 0.005$, Fig. 9A). In contrast, western blot analyses demonstrated that protein levels were unchanged in two Complex IV subunits, COX I and II (Fig. 9B). This deficiency of Complex IV activity in frataxin-deficient cells, without an alteration in the protein level of subunit I or II, is consistent with the idea that decreased heme *a* is available for cytochrome oxidase.

DISCUSSION

Frataxin-deficient mouse tissues exhibit mitochondrial-specific transcriptional inhibition

We microarrayed frataxin deficient in mouse hearts and liver, which exhibit pathology (2) (M. Ristow, unpublished data). We observed that significantly down-regulated transcripts outnumbered significantly up-regulated transcripts by an average of 2 : 1 (Table 1). Thus, frataxin deficiency has an overall inhibitory effect on significantly altered transcripts.

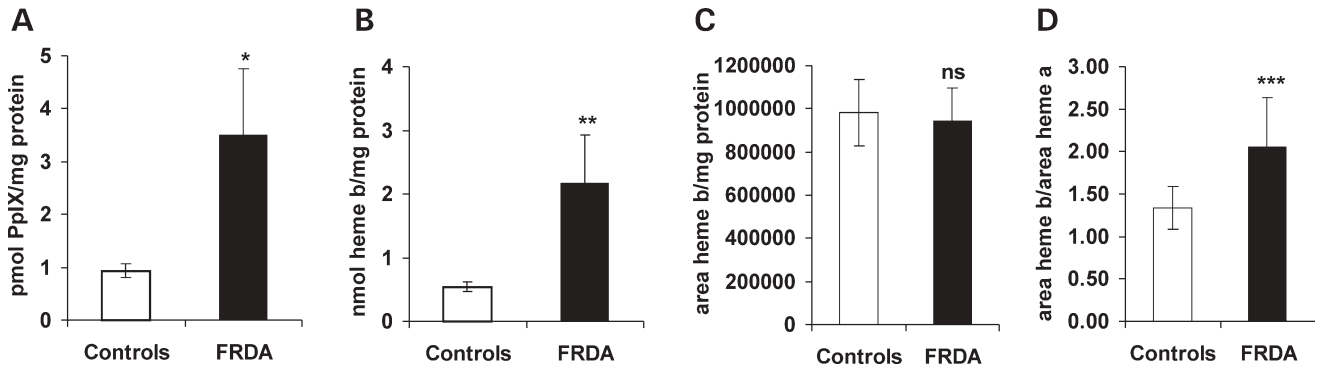

Figure 4. Comparison of protoporphyrin IX, heme b and heme a levels in control and FRDA lymphoblasts. HPLC analysis was used to examine the levels of three compounds in the heme biosynthetic pathway. (**A**) Cellular PpIX levels; (**B**) total cell extract heme *b* levels; (**C**) mitochondrial heme *b* levels expressed as area under the curve/mg protein; (**D**) mitochondrial heme *b* : heme *a* ratio, area/area. The mean values of three experiments using four controls and four FRDA mutants (A and B) or three controls and three FRDA mutants (C and D) are shown. Error bars represent 2 SEM. PpIX, protoporphyrin IX. Statistical analysis was performed by the Student's *t*-test. $^{*}P < 0.005$; $^{**}P < 0.0005$; ns, not significant; $^{***}P < 0.05$.

Onto-Express software was used to analyze the lists of significantly altered genes. Onto-Express sorts a list of significantly altered genes into categories on the basis of cellular compartment, bioprocess or molecular function and then determines whether the distribution of categories is non-random. This analysis overwhelmingly supported the notion that the primary transcriptional effect of frataxin deficiency was on mitochondrial-specific transcripts (Table 2). Of the 54 transcripts identified as mitochondrial specific, 44/54 (81%) were down-regulated, further supporting the notion that the frataxin deficiency produces a mitochondrial-specific transcriptomal inhibition. Thus, frataxin deficiency produces a repressive transcriptional effect, which is significantly mitochondrial. One question provoked by the analysis is what causes the inhibition of mitochondrial genes and functions.

The broadest transpecies and transcellular consequences of frataxin deficiency are down-regulation of coproporphyrinogen oxidase and MTCP-1

In order to determine the most consistent consequences of frataxin deficiency, we compared all microarray experiments we have carried out in mouse and human cells. Next to frataxin, the most frequent significantly decreased transcripts were those of coproporphyrinogen oxidase CPOX and MTCP1. In an earlier microarray study of human cells, the transcript encoding the mitochondrial iron–sulfur repair protein rhodanese scored very highly. It also scored well in this broader study, but not in as many samples as the CPOX and MTCP1 transcripts. Coproporphyrinogen oxidase has been previously described as a control point in heme biosynthesis (42), and MTCP1 is a mitochondrial protein of (currently) unknown function. Our BLASTP analysis shows that MTCP1 is related to yeast COX23 and COX17, which are thought to function as mitochondrial metallochaperones (Fig. 7).

Frataxin-dependent effects on heme flux and metabolites

The microarray data indicated a consistent transcriptional effect of frataxin deficiency on the heme pathway, and this was further confirmed by QRTPCR studies on heme related transcripts in 3, 5, and 10 week hearts (Fig. 1) and at the biochemical level. We observed that frataxin-deficient lymphoblasts were transiently and significantly protected from aminolevulinate-dependent phototoxicity in a time-dependent manner, consistent with the defect in CPOX observed at the transcriptional level (Fig. 3). We observed increased PpIX in mutants, which is consistent with a defect later in the heme pathway, and although total cellular heme *b* levels were also increased by about the same amount, mitochondrial heme *b* levels were not significantly increased in mutants. Furthermore, mitochondrial heme *a* levels were significantly decreased relative to the (unchanged) mitochondrial heme *b* in mutants (Fig. 4). Thus, frataxin deficiency produces no significant alteration in mitochondrial heme *b* levels, but does decrease heme *a* levels. Consistent with the decrease in heme *a* levels, cytochrome oxidase activity was decreased, even though cytochrome oxidase subunits were not, as expected if the deficiency was a result of decreased heme *a* loading of cytochrome oxidase (Fig. 8), and cytochrome *c* levels were also decreased.

The simplest explanation of all the data is that frataxin deficiency causes a defect subsequent to PpIX synthesis, which results in deficiencies of both heme *a*, which reduces the activity of cytochrome oxidase, and heme *c*, which results in decreased heme per cytochrome *c* molecule. It may be that the induction of Complex III we observed is an adaptation to decreased cytochrome oxidase activity and cytochrome *c*. In addition, the reduced availability of heme *a* may be what inhibits the transcription of the COX17/23 homolog MTCP1, which may then affect cytochrome oxidase activity.

A novel possibility suggested by the data is that frataxin may affect the specificity of metallation by ferrochelatase. This idea is supported by the observation that Zn-chelatase activity is increased in mutants, whereas Fe-chelatase activity is unchanged (Fig. 5). The idea of frataxin as an "iron chaperone" for aconitase (18) and for ferrochelatase (33) has received support. If frataxin deficiency causes decreased metal specificity, then insertion of incorrect metals into hemes may decrease the insertion of these incorrectly metallated hemes into hemoproteins. Our observations of

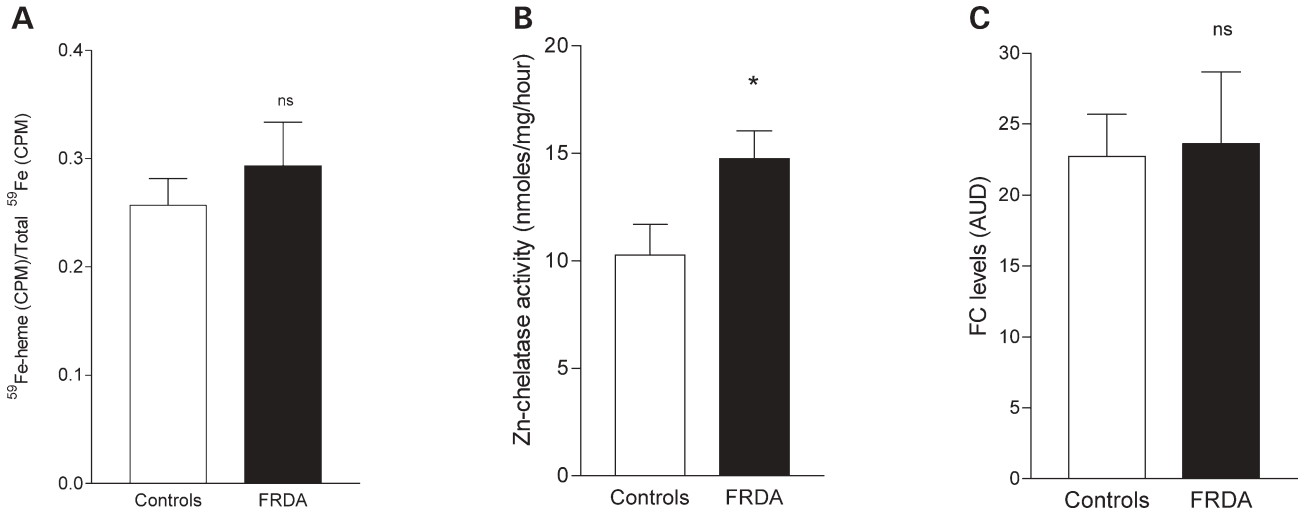

Figure 5. Zinc-chelatase activity, but not ferrochelatase activity or expression, is significantly increased in FRDA cells. (**A**) Fe-chelatase activity is calculated as ratio between the amount of ^{59}Fe inserted in heme and the total ^{59}Fe. A 10 μl of lysate corresponding to 100 μg of mitochondrial protein were used per assay. Heme synthesis reaction was started by adding 5 μl of 100 mM ascorbate and 0.1 μCi of $^{59}FeCl_3$. (**B**) Zn-chelatase activity was measured fluorimetrically by the appearance of Zn–PpIX; fluorescence at 580 nm was read directly after excitation at 450 nm. (**C**) Ferrochelatase levels by densitometry analysis. AUD, arbitrary units of density. Results are expressed as mean ± SEM of at least two experiments in duplicate for three controls and three FRDA mutants. Statistical analysis was performed by the Student's *t*-test. $^*P < 0.05$; ns, not significant.

decreased heme *c* per cytochrome *c* molecule are consistent with this idea. Previous studies of in frataxin-deficient yeast have shown an up-regulation of Zn-chelatase activity (33) and down-regulation of Fe-chelatase activity (34), however, no down-regulation of Fe-chelatase activity was observed in frataxin-siRNA-treated mammalian cells (25).

The other possibility suggested by the data is that frataxin supports the activity of the FeS enzyme adrenodoxin, which catalyzes the first step of the conversion of heme *o* to heme *a*. In this case, frataxin deficiency should lead to decreased adrenodoxin activity, decreased heme *a* levels (which we observe), and then decreased cytochrome oxidase activity, which is likely to feed back and inhibit multiple mitochondrial functions. Pharmacologically induced heme deficiency has previously been shown to cause a preferential loss of cytochrome oxidase activity (53). Further studies should clarify this issue.

Frataxin deficiency inhibits MTCP1 levels

MTCP1 levels were consistently decreased as a consequence of frataxin deficiency in mutant mouse hearts and human lymphoblasts and fibroblasts. We demonstrate by amino acid homology that MTCP1 has similarity to the metallochaperones COX23 and COX17, and we demonstrated decreased cytochrome oxidase activity in the presence of similar amounts of subunits I and II (Fig. 9), consistent with decreased heme insertion into cytochrome oxidase. The simplest rationalization of our data is that frataxin supports the biosynthesis of heme *a*, which then positively regulates MTCP1. The converse is that under conditions of frataxin deficiency, heme *a* deficiency occurs, which decreases heme insertion into cytochrome oxidase, and thus cytochrome oxidase activity, which should be especially important to the aerobic function of the heart.

Sharing of heme alterations among porphyrias and ataxias

Although we have demonstrated that frataxin deficiency causes alterations in transcripts and flux and heme metabolites levels in mammalian cells, we have not proven that it is these alterations that cause the neurodegeneration and cardiac dysfunction that occur in the disease. However, there are multiple connections between heme alterations and ataxia. Taketani *et al.* (54) demonstrated that ferrochelatase expression was regulated by expression of the mitochondrial iron/heme transport gene ABC7, mutations in which cause X-linked sideroblastic anemia and ataxia (55,56). Although porphyric symptoms have not been reported in FRDA patients, a defect in the conversion of PpIX to heme in Friedreich's patients was reported as early as 1979, although this was before identification of the frataxin gene (57). Thus, the heme pathway alterations we demonstrate in human FRDA lymphoblasts could be on the same pathophysiological pathway as the neuro- and cardiodegeneration observed in the disease.

Implications for treatment and therapy

There are multiple implications of these results for treatment of patients with FRDA. Benzodiazepine drugs are known to antagonize the activity of coproporphyrinogen oxidase (58,59), whose transcript is inhibited in FRDA patient cells and frataxin-deficient mice, so the use of these drugs should probably be avoided in these patients. Steroid therapy, which stimulates the heme pathway, might also cause problems, given the apparent inhibition of a step subsequent to PpIX synthesis, and the buildup of toxic PpIX in mutants. It is hoped that a better understanding of heme metabolism in FRDA will lead to better patient outcomes.

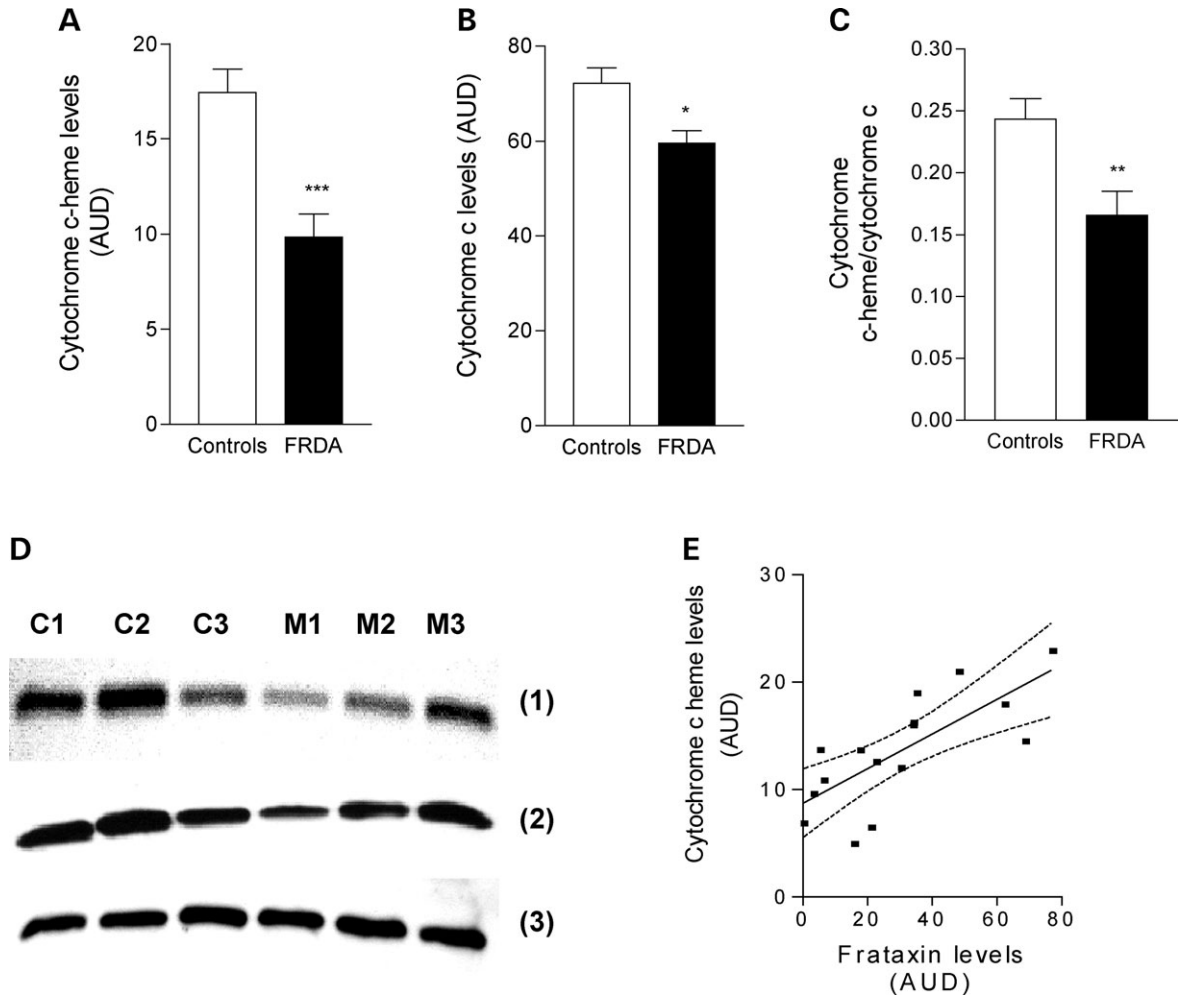

Figure 6. Frataxin specifies cytochrome *c* specific heme levels. (**A**) Densitometry of cytochrome *c* heme (heme *c*). (**B**) Densitometry of cytochrome *c* protein. (**C**) Decreased heme/cytochrome *c* ratio in mutants, $^{**}P \leq 0.01$. (**D**) Representative SDS–PAGE stained with (1) *o*-dianisidine; (2) western blot of cytochrome *c*; (3) western blot of cytochrome oxidase subunit II on same lysates as loading control. A 30 μg of mitochondrial proteins were loaded in each lane. (**E**) Direct correlation between frataxin expression and cytochrome *c* heme levels ($r^2 = 0.547$; $P = 0.0011$). Each dot represents a single sample. C, control; M, mutant; AUD, arbitrary units of densitometry. The results are expressed as mean ± SE of at least two experiments for three controls and three FRDA mutant cell lines. Statistical analysis was performed by the Student's *t*-test. $^{*}P < 0.05$; $^{**}P < 0.05$; $^{***}P < 0.001$.

MATERIALS AND METHODS

Biochemical reagents were purchased from Sigma (St Louis, MO, USA), Invitrogen (Carlsbad, CA, USA) or Bio-Rad (Hercules, CA, USA). Microarray chips were purchased from Affymetrix (Santa Clara, CA, USA).

Cell culture

All cells were maintained at 37°C in a humidified atmosphere containing 5% CO_2. Lymphocytes were grown in RPMI 1640 supplemented with 500 mg/l glutamate, 1 mM sodium pyruvate, 50 μg/ml uridine, 100 μM non-essential amino acids (Invitrogen, Carlsbad, CA, USA), 20% FBS and penicillin/streptomycin. HL-1 cells were grown in MEM alpha modification medium supplemented with 10% FBS, 50 μg/ml endothelial cell growth supplement (Upstate Biotechnology, Lake Placid, NY, USA), 10 μg/ml insulin (Invitrogen), an additional 100 μM non-essential amino acids, 100 U/ml penicillin, 100 μg/ml streptomycin, 1 μM retinoic acid and 100 μM norepinephrine in plastic flasks coated with 12.5 μg/ml fibronectin and 0.02% gelatin. NT2 cells were grown in DMEM supplemented with 10% FBS, 50 μg/ml uridine, 1 mM sodium pyruvate, 2 mM glutamine and 40 μg/ml gentamycin.

siRNA transfections

HL-1 cells were grown to 40–70% confluency in complete medium without antibiotics. Two hundred nanomolar of siRNA (frataxin, GCA GAC CCC AAA CAA GCA AdTdT), Oligofectamine (Invitrogen) transfection agent and Opti-MEM(Invitrogen) were mixed and incubated at room temperature for 15–20 min. The mixture was added to the cells for 4 h followed by adding growth medium containing 30% FBS. Cells were incubated 30 h and then harvested.

A

```
                95   100       110       120       130       140       150       165
hMTCP1   (1) ---MPQKDPCQKQACEIQKCLQANSYMESKCQAVIQELRKCCAQYPKGRSVVCSGFEKEEEENLTRKSASK
yCOX23  (95) KADSQYYDPCEESSKLSFQCLERNDYDRSKCQEYFDAYRECKKQWLTARRKNRQCWE------------
Consensus          DPC   A     CL  N Y  SKCQ      R C  QW  AR      FE
```

B

Sequence	BLASTP E-value	Distance Score
yCOX23	0.004	70
yCOX17	7.5	82
yMRP10	1.5	82
yMRS3	-	88
yMRS4	-	85
ySCO1	-	88
yHht2p	-	87

C

Figure 7. MTCP1 homologies to yeast COX assembly proteins. (**A**) Sequence alignment of human MTCP1 and yeast COX23. Numbers in parentheses indicate amino acid position relative to start codon. Shaded areas indicate identity and boxes indicate conservation. (**B**) Relative ranking of various COX assembly proteins and a yeast histone protein compared to human MTCP1. Distance values were determined using the Align-X subroutine of Vector NTI. (**C**) Structural representations of COX17 (left), $P8^{MTCP1}$ (center) and both (right).

Microarray

Mouse total RNA was extracted using Tri-Reagent (Sigma) and further purified using RNeasy (Qiagen, Valencia, CA, USA). RNA was labeled for hybridization to the microarray chips, according to the manufacturer's recommendations. Mouse hearts (three knockouts and three controls per time point) and HL-1 cardiocyte siRNA (three transfections and one untransfected control) were analyzed using the Affymetrix U74Av2 chip. Mouse livers (four knockouts and four controls) were analyzed using the MOE430 chip set.

Data were analyzed individually for each sample type using dChip. Within each group, samples were normalized to the median intensity chip and fluorescence values generated using the perfect match-only model. Probesets with a pCall $>40\%$ and $P < 0.05$ were considered significantly altered. Frataxin met these criteria and was down-regulated in all samples except the 3-month liver knockouts. Western blot and RT–PCR analyses confirmed the knockout (data not shown).

Updated annotations and orthologs were obtained from the NetAffx database and multi-sample analysis performed by combining the dChip lists using Excel. Expression data for U74Av2 probesets were tabulated, then resorted by gene name. As many genes were represented by multiple probesets, redundant entries or those with expression in opposite directions within a single sample were eliminated. Liver knockout expression data (MOE430 chip set) were then added in, the combined listed sorted by gene name and redundant/opposite expression entries were again eliminated.

Significantly, altered probesets were categorized using Onto-Express (38). The false discovery rate method was used to correct for errors generated by multiple *t*-tests.

Blue light sensitivity

Lymphoblasts were grown as earlier, except in RPMI media lacking Phenol red. ALA was diluted to 20 mM in phosphate buffered saline and the pH adjusted to 7.0. Prior to each experiment, cells were switched to medium containing 1% serum and 100 000 cells per well were plated in 24-well plates. The cells were fed with 300 μM ALA, incubated for 0–20 min then exposed to 400–410 nm light (DUSA Pharmaceuticals, Tarrytown, NY, USA) for 5 min. To control for heat, temperature, humidity and CO_2 effects, no light controls were covered with aluminum foil and placed on the light box alongside exposed samples. An equal volume of medium containing 20% FBS was added to each well after exposure, returning the samples to their original serum level. Cells were then incubated overnight and counted on a ViCell cell counter (Beckman Coulter, Miami, FL, USA).

Mitochondria isolation

Mitochondria were isolated from lymphoblasts following the method of Trounce *et al.* (60). Approximately 1×10^9 cells were harvested by centrifugation and the pellet was re-suspended with 4 ml of isolation buffer (210 mM mannitol, 70 mM sucrose, 1 mM EGTA and 5 mM HEPES, pH 7.2) per

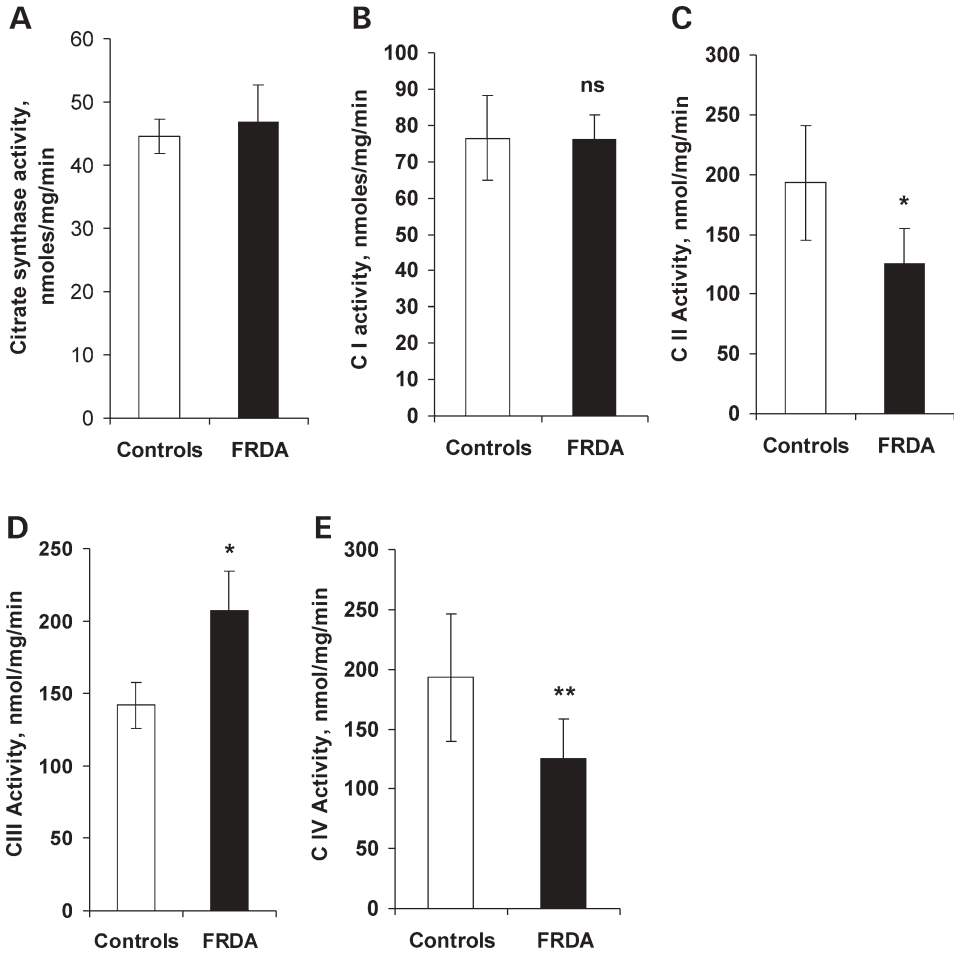

Figure 8. Effects of decreased frataxin levels on Complexes I–IV. Assays were performed using mitochondrial isolates from human lymphoblasts. (**A**) Complex I activity; (**B**) Complex II activity; (**C**) Complex III activity; (**D**) Complex IV activity. The results are expressed as mean ± 2 SEM of two experiments for three controls and three mutant cell lines (B and D) or three controls and two mutants (A and C). Statistical analysis was performed by the Student's *t*-test. ns, not significant; $^{*}P < 0.05$; $^{**}P < 0.005$.

gram of packed cells and treated with a final concentration of 0.3 mg/ml digitonin for 2 min with swirling. After differential centrifugation, the final pellet was suspended with 0.1 ml of isolation buffer per gram of starting cells, giving a protein concentration of approximately 8–12 mg/ml. For determination of mitochondrial protein concentration, 5 μl of the mitochondrial suspension was diluted 1 : 20 in double distilled water and the protein concentration was estimated using the Bradford assay (Bio-Rad).

Western blot analysis

Mitochondria were lysed in 50 mM Tris, pH 8.0, 100 mM NaCl, 1 mM EDTA, 1 mM PMSF, 10 μg/ml aprotinin, 10 μg/ml leupeptin, 1% IGEPAL CA-630 (Sigma), at 4°C for 30 min and insoluble material removed by centrifugation. Protein concentration was estimated using the Bradford assay (Bio-Rad). Equal amounts of lysates (30 μg) were resolved on a 15% SDS–polyacrylamide gel and then transferred to a PVDF membrane (Millipore, Bedford, MA, USA) by electroblotting. After blocking with 4% non-fatdry milk, the blot was incubated with anti-frataxin polyclonal antibody, anti-cytochrome *c*, anti-COX I or anti-COXII and was developed with AP-conjugated secondary antibodies using a chemiluminescent substrate.

Zinc-chelatase activity assay

Zinc-chelatase activity was measured fluorimetrically (61) in permealized pure mitochondria (20 μg) recording the fluorescence intensity of Zn–PpIX (exc. 420 nm; em. 587 nm). The incubation medium was: 50 mM Mes/15 mM Mops/70 mM Tris, pH 5.5, 50 μM protoporphyrin, 200 μM zinc acetate, 1% Triton, 1 mM palmitate and 1 mM DTT. Pure Zn–PpIX was used to calibrate the assay.

Determination of heme synthesis in mitochondrial lysates

Isolated mitochondria were lysed in 1% dodecylmaltoside in 40 mM HEPES/KOH, pH 7.4, 150 mM NaCl and 10% glycerol for 30 min at 0°C. Aggregates were removed by centrifugation

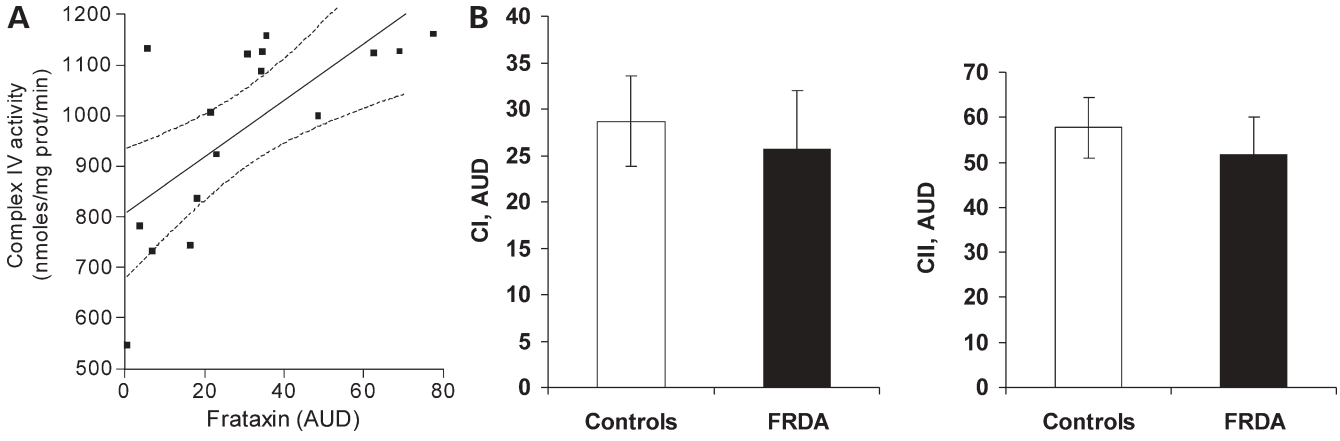

Figure 9. Decreased frataxin levels results in decreased Complex IV (COX) activity but not in decreased expression of COX I and II subunits. **(A)** Linear regression analysis of frataxin expression versus Complex IV activity demonstrates a significant direct correlation between the two variables ($r^2 = 0.4717$, $P = 0.0033$). (**B**) No significant difference was found in the expression of Complex IV subunits I and II between mutants and controls, and no significant correlation with frataxin expression was observed. The results are expressed as the average of at least two experiments for three controls and three FRDA mutant cell lines. Error bars indicate SEM.

at 10 000 r.p.m. for 10 min at 4°C. The amount of mitochondrial lysate corresponding to 100 μg of mitochondrial protein was used to evaluate the insertion of iron into PPIX in a 500 μl standard assay as described (34,62), using a buffer containing 40 mM HEPES/KOH, pH 7.4, 50 mM NaCl, 2 mM NADH and 1 μM deuteroporphyrin. The iron insertion reaction was started by adding 1 mM ascorbate and 0.1 μCi of $^{59}FeCl_3$, incubated for 10 min at 25°C and stopped with 25 μl of 10 mM $FeCl_3$ in 5 N HCl. The mixture was then extracted with 500 μl of butyl acetate and 200 μl of the organic phase counted in a Gamma 5000 counter.

Mitochondrial enzyme activity assays

The activities of complexes I–IV of the respiratory chain were evaluated in mitochondrial isolates as previously described.

NADH : ubiquinone oxidoreductase activity was measured in three controls and two FRDA lymphoblast lines measuring the decrease in absorbance due to the oxidation of NADH at 340 nm, with 425 nm as the reference wavelength according to the method of Birch-Machin and Turnbull (63) with minor modifications. The assay medium consisted in 25 mM KH_2PO_4, pH 7.2, 5 mM $MgCl_2$ and 2 mM KCN. NADH (0.13 mM), ubiquinone$_1$ (65 μM) and antimycin A (2 μg/ml) were added to the assay medium and the absorbance recorded for 1 min at 30°C. Mitochondria (previously freeze-thawed three times in hypotonic media), treated or untreated with 2 μg/ml rotenone for 5 min, were added and the absorbance was measured for 3 min. Complex I activity was considered the rotenone-sensitive NADH : ubiquinone oxidoreductase activity.

Succinate dehydrogenase, cytochrome *c* oxidase and citrate synthase were evaluated in mitochondria isolated from two control and two FRDA patients lymphoblasts.

Succinate dehydrogenase activity was measured by following the reduction of 2,6-dichlorophenolindophenol at 600 nm as described (63).

Cytochrome *c* reductase activity was measured using a variation of the single wavelength spectrophotometric assay previously described (64). The reduction of cytochrome *c* was monitored at 550 nm for 2 min at 30°C. Mitochondria (50 μg) were incubated in a mixture containing 25 μM KH_2PO_4, pH 7.2, 200 μM NADH, 40 μM KCN, 100 μM cytochrome *c* and 1 μM rotenone. Activity was measured by calculating the change in absorbance ±2 μg/ml antimycin A using $\epsilon = 18.5$.

Cytochrome oxidase activity was evaluated by the single wavelength spectrophotometric assay previously described (65) with some modifications. Mitochondria (1.5 μg) were incubated with 2.5 mM dodecylmaltoside in 0.17 M KH_2PO_4, pH 7.0, for 3′ at 30°C, and, after recording the baseline, the reaction was started with 10 mM reduced cytochrome *c*. The COX activity was calculated from the pseudo-linear rate of cytochrome *c* oxidation at 550 nm.

Citrate synthase was evaluated as described (66), following the disappearance of 5,5′-dithiobis(2-nitrobenzoic acid) at 412 nm.

Respiratory complex activity assays

Cytochrome oxidase activity was evaluated by the single wavelength spectrophotometric assay previously described (65) with some modifications. Mitochondria (1.5 μg) were incubated with 2.5 mM dodecylmaltoside in 0.17 M KH_2PO_4, pH 7.0, for 3′ at 30°C, and, after recording the baseline, the reaction was started with 10 mM reduced cytochrome *c*. The COX activity was calculated from the pseudo-linear rate of cytochrome *c* oxidation at 550 nm.

Heme staining of cytochrome *c*

Mitochondrial extracts were separated on a 15% SDS–PAGE. Heme staining was performed as previously described (67).

HPLC analysis of coproporphyrin III, protoporphyrin IX and heme

A Luna C-18, 4.6 × 100 mm, 5 μm particle size column was used. Standards were prepared from coproporphyrin III, protoporphyrin IX, hemin (Frontier Scientific, Logan, UT, USA) and heme *a* (purified by Dr Eric Hegg, University of Utah and provided as a gift by Dr Brian Gibney, Columbia University). All data were analyzed using Millenium software (Waters, Milford, MA, USA).

Lymphoblasts were washed twice with ice-cold PBS and lysed with 5% HCl in acetone. After 20 min on ice, supernatants were collected for HPLC analysis after centrifugation at 18 000*g* for 3 min. Coproporphyrin III, protoporphyrin IX and heme were eluted using a step gradient of 10 min at 60% buffer A (0.5% trifluoroacetic acid in water) and 40% buffer B (0.5% trifluoroacetic acid in acetonitrile), 30 min at 50% buffer A and 10 min at 0% buffer A. The flow rate was 0.5 ml/min, and peaks were monitored at 405 nm.

Mitochondrial proteins (100 μg) were lysed with 5% HCl in acetone for 20 min on ice, centrifuged at 18 000*g* for 5 min and supernatants collected for analysis. The gradient used to measure heme *b* (hemin) and heme *a* was from 100% buffer A (35% acetonitrile, 0.08% trifluoroacetic acid) and 0% buffer B (0.08% trifluoroacetic acid in acetonitrile) to 0% A and 100% B over 45 min with a flow rate of 1.0 ml/min. Peaks were monitored at 405 nm.

ACKNOWLEDGEMENTS

Fariba Ashkan Far's help with QRTPCR and Dr Ben Edwards' help with blue light experiments are gratefully acknowledged. M.R. solely provided samples derived from unpublished mouse models for this work. This work was supported by United States Public Health Services grants AG11967, AG16719, EY12245, AG23311 (to G.A.C.) and the Deutsche Forschungsgemeinschaft and the Fritz-Thyssen-Stiftung (to M.R.).

Conflict of Interest statement. None declared.

REFERENCES

1. Pandolfo, M. (2002) Iron metabolism and mitochondrial abnormalities in Friedreich ataxia. *Blood Cells Mol. Dis.*, **29**, 536–547; discussion 548–552.
2. Puccio, H., Simon, D., Cossee, M., Criqui-Filipe, P., Tiziano, F., Melki, J., Hindelang, C., Matyas, R., Rustin, P. and Koenig, M. (2001) Mouse models for Friedreich ataxia exhibit cardiomyopathy, sensory nerve defect and Fe–S enzyme deficiency followed by intramitochondrial iron deposits. *Nat. Genet.*, **27**, 181–186.
3. Seznec, H., Simon, D., Monassier, L., Criqui-Filipe, P., Gansmuller, A., Rustin, P., Koenig, M. and Puccio, H. (2004) Idebenone delays the onset of cardiac functional alteration without correction of Fe–S enzymes deficit in a mouse model for Friedreich ataxia. *Hum. Mol. Genet.*, **13**, 1017–1024.
4. Campuzano, V., Montermini, L., Molto, M.D., Pianese, L., Cossee, M., Cavalcanti, F., Monros, E., Rodius, F., Duclos, F., Monticelli, A. *et al.* (1996) Friedreich's ataxia: autosomal recessive disease caused by an intronic GAA triplet repeat expansion. *Science*, **271**, 1423–1427.
5. Ohshima, K., Montermini, L., Wells, R.D. and Pandolfo, M. (1998) Inhibitory effects of expanded GAA.TTC triplet repeats from intron I of the Friedreich ataxia gene on transcription and replication *in vivo*. *J. Biol. Chem.*, **273**, 14588–14595.
6. Sakamoto, N., Chastain, P.D., Parniewski, P., Ohshima, K., Pandolfo, M., Griffith, J.D. and Wells, R.D. (1999) Sticky DNA: self-association properties of long GAA.TTC repeats in R.R.Y triplex structures from Friedreich's ataxia. *Mol. Cell*, **3**, 465–475.
7. Sakamoto, N., Larson, J.E., Iyer, R.R., Montermini, L., Pandolfo, M. and Wells, R.D. (2001) GGA*TCC-interrupted triplets in long GAA*TTC repeats inhibit the formation of triplex and sticky DNA structures, alleviate transcription inhibition, and reduce genetic instabilities. *J. Biol. Chem.*, **276**, 27178–27187.
8. Sakamoto, N., Ohshima, K., Montermini, L., Pandolfo, M. and Wells, R.D. (2001) Sticky DNA, a self-associated complex formed at long GAA*TTC repeats in intron 1 of the frataxin gene, inhibits transcription. *J. Biol. Chem.*, **276**, 27171–27177.
9. Lamont, P.J., Davis, M.B. and Wood, N.W. (1997) Identification and sizing of the GAA trinucleotide repeat expansion of Friedreich's ataxia in 56 patients. Clinical and genetic correlates. *Brain*, **120**, 673–680.
10. Filla, A., De Michele, G., Cavalcanti, F., Pianese, L., Monticelli, A., Campanella, G. and Cocozza, S. (1996) The relationship between trinucleotide (GAA) repeat length and clinical features in Friedreich ataxia. *Am. J. Hum. Genet.*, **59**, 554–560.
11. Durr, A., Cossee, M., Agid, Y., Campuzano, V., Mignard, C., Penet, C., Mandel, J.L., Brice, A. and Koenig, M. (1996) Clinical and genetic abnormalities in patients with Friedreich's ataxia. *N. Engl. J. Med.*, **335**, 1169–1175.
12. Montermini, L., Richter, A., Morgan, K., Justice, C.M., Julien, D., Castellotti, B., Mercier, J., Poirier, J., Capozzoli, F., Bouchard, J.P. *et al.* (1997) Phenotypic variability in Friedreich ataxia: role of the associated GAA triplet repeat expansion. *Ann. Neurol.*, **41**, 675–682.
13. Monros, E., Molto, M.D., Martinez, F., Canizares, J., Blanca, J., Vilchez, J.J., Prieto, F., de Frutos, R. and Palau, F. (1997) Phenotype correlation and intergenerational dynamics of the Friedreich ataxia GAA trinucleotide repeat. *Am. J. Hum. Genet.*, **61**, 101–110.
14. Lill, R. and Muhlenhoff, U. (2005) Iron–sulfur-protein biogenesis in eukaryotes. *Trends Biochem. Sci.*, **30**, 133–141.
15. Yoon, T. and Cowan, J.A. (2003) Iron–sulfur cluster biosynthesis. Characterization of frataxin as an iron donor for assembly of [2Fe–2S] clusters in ISU-type proteins. *J. Am. Chem. Soc.*, **125**, 6078–6084.
16. Yoon, T. and Cowan, J.A. (2004) Frataxin-mediated iron delivery to Ferrochelatase in the final step of heme biosynthesis. *J. Biol. Chem.*, **279**, 25943–25946.
17. Park, S., Gakh, O., O'Neill, H.A., Mangravita, A., Nichol, H., Ferreira, G.C. and Isaya, G. (2003) Yeast frataxin sequentially chaperones and stores iron by coupling protein assembly with iron oxidation. *J. Biol. Chem.*, **278**, 31340–31351.
18. Bulteau, A.L., O'Neill, H.A., Kennedy, M.C., Ikeda-Saito, M., Isaya, G. and Szweda, L.I. (2004) Frataxin acts as an iron chaperone protein to modulate mitochondrial aconitase activity. *Science*, **305**, 242–245.
19. Duby, G., Foury, F., Ramazzotti, A., Herrmann, J. and Lutz, T. (2002) A non-essential function for yeast frataxin in iron–sulfur cluster assembly. *Hum. Mol. Genet.*, **11**, 2635–2643.
20. Muhlenhoff, U., Richhardt, N., Ristow, M., Kispal, G. and Lill, R. (2002) The yeast frataxin homolog Yfh1p plays a specific role in the maturation of cellular Fe/S proteins. *Hum. Mol. Genet.*, **11**, 2025–2036.
21. Muhlenhoff, U., Gerber, J., Richhardt, N. and Lill, R. (2003) Components involved in assembly and dislocation of iron–sulfur clusters on the scaffold protein Isu1p. *EMBO J.*, **22**, 4815–4825.
22. Gerber, J., Muhlenhoff, U. and Lill, R. (2003) An interaction between frataxin and Isu1/Nfs1 that is crucial for Fe/S cluster synthesis on Isu1. *EMBO Rep.*, **4**, 906–911.
23. Ramazzotti, A., Vanmansart, V. and Foury, F. (2004) Mitochondrial functional interactions between frataxin and Isu1p, the iron–sulfur cluster scaffold protein, in *Saccharomyces cerevisiae*. *FEBS Lett.*, **557**, 215–220.
24. Tan, G., Napoli, E., Taroni, F. and Cortopassi, G. (2003) Decreased expression of genes involved in sulfur amino acid metabolism in frataxin-deficient cells. *Hum. Mol. Genet.*, **12**, 1699–1711.
25. Stehling, O., Elsasser, H.P., Bruckel, B., Muhlenhoff, U. and Lill, R. (2004) Iron–sulfur protein maturation in human cells: evidence for a function of frataxin. *Hum. Mol. Genet.*, **13**, 3007–3015.
26. Adamec, J., Rusnak, F., Owen, W.G., Naylor, S., Benson, L.M., Gacy, A.M. and Isaya, G. (2000) Iron-dependent self-assembly of recombinant yeast frataxin: implications for Friedreich ataxia. *Am. J. Hum. Genet.*, **67**, 549–562.

27. Cavadini, P., O'Neill, H.A., Benada, O. and Isaya, G. (2002) Assembly and iron-binding properties of human frataxin, the protein deficient in Friedreich ataxia. *Hum. Mol. Genet.*, **11**, 217–227.
28. Bou-Abdallah, F., Adinolfi, S., Pastore, A., Laue, T.M. and Dennis Chasteen, N. (2004) Iron binding and oxidation kinetics in frataxin CyaY of *Escherichia coli*. *J. Mol. Biol.*, **341**, 605–615.
29. O'Neill, H.A., Gakh, O. and Isaya, G. (2005) Supramolecular assemblies of human frataxin are formed via subunit–subunit interactions mediated by a non-conserved amino-terminal region. *J. Mol. Biol.*, **345**, 433–439.
30. O'Neill, H.A., Gakh, O., Park, S., Cui, J., Mooney, S.M., Sampson, M., Ferreira, G.C. and Isaya, G. (2005) Assembly of human frataxin is a mechanism for detoxifying redox-active iron. *Biochemistry*, **44**, 537–545.
31. He, Y., Alam, S.L., Proteasa, S.V., Zhang, Y., Lesuisse, E., Dancis, A. and Stemmler, T.L. (2004) Yeast frataxin solution structure, iron binding, and ferrochelatase interaction. *Biochemistry*, **43**, 16254–16262.
32. Nair, M., Adinolfi, S., Pastore, C., Kelly, G., Temussi, P. and Pastore, A. (2004) Solution structure of the bacterial frataxin ortholog, CyaY: mapping the iron binding sites. *Structure (Camb.)*, **12**, 2037–2048.
33. Lesuisse, E., Santos, R., Matzanke, B.F., Knight, S.A., Camadro, J.M. and Dancis, A. (2003) Iron use for haem synthesis is under control of the yeast frataxin homologue (Yfh1). *Hum. Mol. Genet.*, **12**, 879–889.
34. Lange, H., Muehlenhoff, U., Denzel, M., Kispal, G. and Lill, R. (2004) The heme synthesis defect of mutants impaired in mitochondrial iron–sulfur protein biogenesis is caused by reversible inhibition of ferrochelatase. *J. Biol. Chem.*, **279**, 29101–29108.
35. Dailey, H.A., Finnegan, M.G. and Johnson, M.K. (1994) Human ferrochelatase is an iron–sulfur protein. *Biochemistry*, **33**, 403–407.
36. Claycomb, W.C., Lanson, N.A., Jr, Stallworth, B.S., Egeland, D.B., Delcarpio, J.B., Bahinski, A. and Izzo, N.J., Jr. (1998) HL-1 cells: a cardiac muscle cell line that contracts and retains phenotypic characteristics of the adult cardiomyocyte. *Proc. Natl Acad. Sci. USA*, **95**, 2979–2984.
37. Schadt, E.E., Li, C., Ellis, B. and Wong, W.H. (2001) Feature extraction and normalization algorithms for high-density oligonucleotide gene expression array data. *J. Cell. Biochem. Suppl.*, **84**, (Suppl. 37), 120–125.
38. Draghici, S., Khatri, P., Bhavsar, P., Shah, A., Krawetz, S.A. and Tainsky, M.A. (2003) Onto-Tools, the toolkit of the modern biologist: Onto-Express, Onto-Compare, Onto-Design and Onto-Translate. *Nucleic Acids Res.*, **31**, 3775–3781.
39. Liu, G., Loraine, A.E., Shigeta, R., Cline, M., Cheng, J., Valmeekam, V., Sun, S., Kulp, D. and Siani-Rose, M.A. (2003) NetAffx: Affymetrix probesets and annotations. *Nucleic Acids Res.*, **31**, 82–86.
40. Pennacchio, L.A., Lehesjoki, A.E., Stone, N.E., Willour, V.L., Virtaneva, K., Miao, J., D'Amato, E., Ramirez, L., Faham, M., Koskiniemi, M. *et al.* (1996) Mutations in the gene encoding cystatin B in progressive myoclonus epilepsy (EPM1). *Science*, **271**, 1731–1734.
41. Ceru, S., Rabzelj, S., Kopitar-Jerala, N., Turk, V. and Zerovnik, E. (2005) Protein aggregation as a possible cause for pathology in a subset of familial Unverricht-Lundborg disease. *Med. Hypotheses*, **64**, 955–959.
42. Woodard, S.I. and Dailey, H.A. (2000) Multiple regulatory steps in erythroid heme biosynthesis. *Arch. Biochem. Biophys.*, **384**, 375–378.
43. Gupta, A.K. and Ryder, J.E. (2003) Photodynamic therapy and topical aminolevulinic acid: an overview. *Am. J. Clin. Dermatol.*, **4**, 699–708.
44. Stern, M.H., Soulier, J., Rosenzwajg, M., Nakahara, K., Canki-Klain, N., Aurias, A., Sigaux, F. and Kirsch, I.R. (1993) MTCP-1: a novel gene on the human chromosome Xq28 translocated to the T cell receptor alpha/delta locus in mature T cell proliferations. *Oncogene*, **8**, 2475–2483.
45. Madani, A., Soulier, J., Schmid, M., Plichtova, R., Lerme, F., Gateau-Roesch, O., Garnier, J.P., Pla, M., Sigaux, F. and Stern, M.H. (1995) The 8 kDa product of the putative oncogene MTCP-1 is a mitochondrial protein. *Oncogene*, **10**, 2259–2262.
46. Fu, Z.Q., Du Bois, G.C., Song, S.P., Kulikovskaya, I., Virgilio, L., Rothstein, J.L., Croce, C.M., Weber, I.T. and Harrison, R.W. (1998) Crystal structure of MTCP-1: implications for role of TCL-1 and MTCP-1 in T cell malignancies. *Proc. Natl Acad. Sci. USA*, **95**, 3413–3418.
47. Altschul, S.F., Madden, T.L., Schaffer, A.A., Zhang, J., Zhang, Z., Miller, W. and Lipman, D.J. (1997) Gapped BLAST and PSI-BLAST: a new generation of protein database search programs. *Nucleic Acids Res.*, **25**, 3389–3402.
48. Barros, M.H., Johnson, A. and Tzagoloff, A. (2004) COX23, a homologue of COX17, is required for cytochrome oxidase assembly. *J. Biol. Chem.*, **279**, 31943–31947.
49. Hogue, C.W. (1997) Cn3D: a new generation of three-dimensional molecular structure viewer. *Trends Biochem. Sci.*, **22**, 314–316.
50. Leary, S.C., Kaufman, B.A., Pellecchia, G., Guercin, G.H., Mattman, A., Jaksch, M. and Shoubridge, E.A. (2004) Human SCO1 and SCO2 have independent, cooperative functions in copper delivery to cytochrome *c* oxidase. *Hum. Mol. Genet.*, **13**, 1839–1848.
51. Valnot, I., Osmond, S., Gigarel, N., Mehaye, B., Amiel, J., Cormier-Daire, V., Munnich, A., Bonnefont, J.P., Rustin, P. and Rotig, A. (2000) Mutations of the SCO1 gene in mitochondrial cytochrome *c* oxidase deficiency with neonatal-onset hepatic failure and encephalopathy. *Am. J. Hum. Genet.*, **67**, 1104–1109.
52. Glerum, D.M., Shtanko, A. and Tzagoloff, A. (1996) Characterization of COX17, a yeast gene involved in copper metabolism and assembly of cytochrome oxidase. *J. Biol. Chem.*, **271**, 14504–14509.
53. Atamna, H., Liu, J. and Ames, B.N. (2001) Heme deficiency selectively interrupts assembly of mitochondrial complex IV in human fibroblasts: relevance to aging. *J. Biol. Chem.*, **276**, 48410–48416.
54. Taketani, S., Kakimoto, K., Ueta, H., Masaki, R. and Furukawa, T. (2003) Involvement of ABC7 in the biosynthesis of heme in erythroid cells: interaction of ABC7 with ferrochelatase. *Blood*, **101**, 3274–3280.
55. Bekri, S., Kispal, G., Lange, H., Fitzsimons, E., Tolmie, J., Lill, R. and Bishop, D.F. (2000) Human ABC7 transporter: gene structure and mutation causing X-linked sideroblastic anemia with ataxia with disruption of cytosolic iron–sulfur protein maturation. *Blood*, **96**, 3256–3264.
56. Allikmets, R., Raskind, W.H., Hutchinson, A., Schueck, N.D., Dean, M. and Koeller, D.M. (1999) Mutation of a putative mitochondrial iron transporter gene (ABC7) in X-linked sideroblastic anemia and ataxia (XLSA/A). *Hum. Mol. Genet.*, **8**, 743–749.
57. Morgan, R.O., Naglie, G., Horrobin, D.F. and Barbeau, A. (1979) Erythrocyte protoporphyrin levels in patients with Friedreich's and other ataxias. *Can. J. Neurol. Sci.*, **6**, 227–232.
58. Taketani, S., Kohno, H., Okuda, M., Furukawa, T. and Tokunaga, R. (1994) Induction of peripheral-type benzodiazepine receptors during differentiation of mouse erythroleukemia cells. A possible involvement of these receptors in heme biosynthesis. *J. Biol. Chem.*, **269**, 7527–7531.
59. Taketani, S., Kohno, H., Furukawa, T. and Tokunaga, R. (1995) Involvement of peripheral-type benzodiazepine receptors in the intracellular transport of heme and porphyrins. *J. Biochem. (Tokyo)*, **117**, 875–880.
60. Trounce, I.A., Kim, Y.L., Jun, A.S. and Wallace, D.C. (1996) Assessment of mitochondrial oxidative phosphorylation in patient muscle biopsies, lymphoblasts, and transmitochondrial cell lines. *Methods Enzymol.*, **264**, 484–509.
61. Nunn, A.V., Norris, P., Hawk, J.L. and Cox, T.M. (1988) Zinc chelatase in human lymphocytes: detection of the enzymatic defect in erythropoietic protoporphyria. *Anal. Biochem.*, **174**, 146–150.
62. Lange, H., Kispal, G. and Lill, R. (1999) Mechanism of iron transport to the site of heme synthesis inside yeast mitochondria. *J. Biol. Chem.*, **274**, 18989–18996.
63. Birch-Machin, M.A. and Turnbull, D.M. (2001) Assaying mitochondrial respiratory complex activity in mitochondria isolated from human cells and tissues. *Methods Cell Biol.*, **65**, 97–117.
64. Sottocasa, G.L., Kuylenstierna, B., Ernster, L. and Bergstrand, A. (1967) An electron-transport system associated with the outer membrane of liver mitochondria. A biochemical and morphological study. *J. Cell Biol.*, **32**, 415–438.
65. Miro, O., Cardellach, F., Barrientos, A., Casademont, J., Rotig, A. and Rustin, P. (1998) Cytochrome *c* oxidase assay in minute amounts of human skeletal muscle using single wavelength spectrophotometers. *J. Neurosci. Methods*, **80**, 107–111.
66. Srere, P.A. (1969) Citrate synthase. In John M. Lowenstein (ed.), *Methods in Enzymology: Oxidation and Phosphorylation*. Academic Press, New York, pp. 3–11.
67. Schulz, H., Pellicioli, E.C. and Thony-Meyer, L. (2000) New insights into the role of CcmC, CcmD and CcmE in the haem delivery pathway during cytochrome *c* maturation by a complete mutational analysis of the conserved tryptophan-rich motif of CcmC. *Mol. Microbiol.*, **37**, 1379–1388.
68. Moraes, C.T., Diaz, F. and Barrientos, A. (2004) Defects in the biosynthesis of mitochondrial heme c and heme a in yeast and mammals. *Biochim. Biophys. Acta*, **1659**, 153–159.
69. Bertini, I. (2002) Biologically relevant heme cofactors. Vol. 2005. http://www.cerm.unifi.it/CHBIOIN/lez2.htm. Web page retrieved 8/1/2005.